

Dendritic tip selection during solidification of alloys: Insights from phase-field simulations

Qingjie Zhang(张清杰), Hui Xing(邢辉), Lingjie Wang(王灵杰), and Wei Zhai(翟薇)

Citation: Chin. Phys. B, 2024, 33 (**9**): 096103. DOI: 10.1088/1674-1056/ad57ac
Journal homepage: http://cpb.iphy.ac.cn; http://iopscience.iop.org/cpb

What follows is a list of articles you may be interested in

Databases of 2D material-substrate interfaces and 2D charged building blocks

Jun Deng(邓俊), Jinbo Pan(潘金波), and Shixuan Du(杜世萱)
Chin. Phys. B, 2024, 33 (**2**): 026101. DOI: 10.1088/1674-1056/ad0626

Pressure-induced phase transition and electronic structure evolution in layered semimetal $HfTe_2$

Mei-Guang Zhang(张美光), Lei Chen(陈磊), Long Feng(冯龙), Huan-Huan Tuo(拓换换), Yun Zhang(张云), Qun Wei(魏群), and Pei-Fang Li(李培芳)
Chin. Phys. B, 2023, 32 (**8**): 086101. DOI: 10.1088/1674-1056/acd2bf

Definition and expression of non-symmetric physical properties in space for uniaxial crystals

Xiaojie Guo(郭晓杰), Lijuan Chen(陈丽娟), Zeliang Gao(高泽亮), Xin Yin(尹鑫), and Xutang Tao(陶绪堂)
Chin. Phys. B, 2022, 31 (**9**): 096103. DOI: 10.1088/1674-1056/ac4e09

Substitutions of vertex configuration of Ammann-Beenker tiling in framework of Ammann lines

Jia-Rong Ye(叶家容), Wei-Shen Huang(黄伟深), and Xiu-Jun Fu(傅秀军)
Chin. Phys. B, 2022, 31 (**8**): 086101. DOI: 10.1088/1674-1056/ac5981

Temperature-dependent structure and magnetization of $YCrO_3$ compound

Qian Zhao(赵前), Ying-Hao Zhu(朱英浩), Si Wu(吴思), Jun-Chao Xia(夏俊超), Peng-Fei Zhou(周鹏飞), Kai-Tong Sun(孙楷橦), and Hai-Feng Li(李海峰)
Chin. Phys. B, 2022, 31 (**4**): 046101. DOI: 10.1088/1674-1056/ac2b23

Dendritic tip selection during solidification of alloys: Insights from phase-field simulations

Qingjie Zhang(张清杰)[1], Hui Xing(邢辉)[1,2,†], Lingjie Wang(王灵杰)[1], and Wei Zhai(翟薇)[1]

[1] *School of Physical Science and Technology, Northwestern Polytechnical University, Xi'an* 710072, *China*
[2] *Research & Development Institute of Northwestern Polytechnical University in Shenzhen, Shenzhen* 518063, *China*

(Received 15 March 2024; revised manuscript received 20 May 2024; accepted manuscript online 13 June 2024)

The effect of undercooling ΔT and the interface energy anisotropy parameter ε_4 on the shape of the equiaxed dendritic tip has been investigated by using a quantitative phase-field model for solidification of binary alloys. It was found that the tip radius ρ increases and the tip shape amplitude coefficient A_4 decreases with the increase of the fitting range for all cases. The dendrite tip shape selection parameter σ^* decreases and then stabilizes with the increase of the fitting range, and σ^* increases with the increase of ε_4. The relationship between σ^* and ε_4 follows a power-law function $\sigma^* \propto \varepsilon_4^{\alpha}$, and α is independent of ΔT but dependent on the fitting range. Numerical results demonstrate that the predicted σ^* is consistent with the curve of microscopic solvability theory (MST) for $\varepsilon_4 < 0.02$, and σ^* obtained from our phase-field simulations is sensitive to the undercooling when ε_4 is fixed.

Keywords: phase-field simulations, dendritic structure, interface energy anisotropy, tip shape selection parameter

PACS: 61.50.Ah, 81.10.Aj, 02.70.–c, 61.72.–y **DOI:** 10.1088/1674-1056/ad57ac

1. Introduction

Dendrites are a common growth pattern observed during solidification of alloys. Understanding the characteristics and stability of the dendritic tip has been of enduring interest in both the metallurgy and physics communities because the dendrite is not only a typical example of self-organized pattern formation but also has an influence on the mechanical properties of casting parts.[1]

The dendritic tip during solidification is characterized by the steady-state growth velocity V and the tip radius ρ. It is well known that the shape of the dendrite can be approximated as an axisymmetric paraboloid in the vicinity of its tip while the fourth-order polynomial fit motivated by the theory for the width of a non-axisymmetric needle crystal close to the tip can be expressed as $y/\rho = (x/\rho)^2/2 - A_4(x/\rho)^4$, where y and x have the orientations opposite and perpendicular to the dendritic growth direction, respectively, A_4 is the fourth-order amplitude coefficient. The fourth-order polynomial expression, representing the deviation from the isotropic form of the shape, can reduce to a simple parabola when the fourth-order term is omitted. Previous investigations reveal that the parameter A_4 is independent of materials and solidification conditions, yet the experimental and numerical values of A_4 from differ significantly from the theoretical solution.[2]

The tip selection constant $\sigma^* = 2D_l d_0/(\rho^2 V)$[3] can be regarded as a fundamental relationship between the steady-state growth velocity V and the tip radius ρ because it appears to be independent of the solidification conditions at low undercooling, where D_l is the liquid solute diffusivity, and d_0 is the capillary length. Moreover, the tip selection constant is an important input parameter for solidification rate in macroscopic simulation of casting. According to marginal stability criterion (MSC),[3] σ^* has the value of $1/(4\pi^2)$, which is close to the experimental value of 0.0192 for the ground based experiments and 0.0195 for microgravity experiments. Nevertheless, according to microscopic solvability theory (MST),[4] in the limit of vanishing Péclet number, i.e., in the low undercooling regime, σ^* depends upon the interface energy anisotropy parameter ε_4 for a 4-fold crystalline symmetry, yielding a relationship $\sigma^* \propto \varepsilon_4^{7/4}$, where σ^* trends to zero as ε_4 approaches zero, since no steady-state solution exists without anisotropy.

In the last few decades, experimental and numerical investigations have been carried out to further understand the characteristics and stability of the dendritic tip. Chopra *et al.*[5] carried out succinonitrile–acetone (SCN–ACE) experiments over a wide range of undercooling and solute concentrations. Based on their data, Li and Beckermann[6] found that σ^* is relatively independent of the undercooling within the range from $\Delta T = 0.1$ K to 0.9 K, and σ^* is significantly above 0.02, the expected value with strong scatter. Experiments by Melendez and Beckermann[7] on the free dendritic growth of succinonitrile–acetone alloys in undercooled melts demonstrated that the tip selection constant σ^* is verified to be independent of the alloy composition, spanning from 0.0086 mol% to 0.4976 mol%. However, the results indicate a strong dependence of σ^* on the undercooling, ranging from $\Delta T = 0.1$ K to 10 K. Moreover, the fourth-order amplitude coefficient A_4 for the fins close to the dendrite tip equal to 0.004 over the same

†Corresponding author. E-mail: huixing@nwpu.edu.cn

© 2024 Chinese Physical Society and IOP Publishing Ltd

range of undercooling, and it is dissimilar from the value of $1/96$ from MST. In experiments of opaque metal and alloys, σ^* from analysis of micrographs of a quenched Al–Cu sample in directional solidification was determined by Liu *et al.*[8] Although the measured value is 0.0237 ± 0.003, it can be found that the trend of decrease of σ^* with the increase of pulling velocity within the pulling velocity ranging from 20 μm/s to 80 μm/s. Recently, Neumann-Heyme *et al.*[2] applied high-resolution synchrotron radiography and advanced image processing techniques to a thin sample of a solidifying Ga-35 wt.% In alloy for *in situ* measurements of dendrite tip shape selection, and they found that $\sigma^* = 0.0768$ that is consistent with the value from MST when $\varepsilon_4 = 0.015$ and $A_4 = 0.00406$ is in excellent agreement with previous results.[9,10]

The phase-field method has been a powerful technique of choice for simulating dendritic growth during solidification, with numerous notable examples of its success.[11–18] Based on the quantitative phase-field simulations, Karma and Rappel[19] found that σ^* from phase-field simulations is slightly larger than solvability theory predictions for small interface energy anisotropy parameter, while σ^* is significantly larger than solvability theory predictions for large the interface energy anisotropy parameter. Moreover, A_4 is found to be in the range 0.0042 to 0.005[20] in agreement with the tip morphology measurements in succinonitrile.[21] Mullis and his coworker[22,23] conducted phase-field simulations of binary alloy solidification, incorporating coupled heat and solute diffusion. Their findings reveal that σ^* not only varies nonmonotonically with undercooling but also changes as the ratio of thermal diffusivity to solutal diffusivity increases at a fixed undercooling. Therefore, it seems that σ^* is a function of undercooling and it decreases with the increase of the undercooling, even if the calculation of σ^* from numerical simulations strongly depends on the obtained tip radius ρ that is sensitive to the fitting range, as discussed in Ref. [7]. However, the variation of σ^* with the interface energy anisotropy parameter is not clear.

In this paper, we present isothermal quantitative phase-field simulations of alloys coupled with real alloy phase diagrams, focusing specifically on dendritic tip selection during solidification. Our numerical simulations were conducted on the online software platform, PhaseLab V1.0, where the phase diagram can be directly accessed from the Phase Diagram module.

2. Model descriptions and parameter selection

In this paper, we adopt a quantitative phase-field model for alloys,[24] which is combined with a binary phase diagram at a fixed temperature. This model utilizes a nonconserved order parameter that varies continuously but sharply between $+1$ (solid phase) and -1 (liquid phase). Therefore, the contour of $\varphi = 0$ can be interpreted as representing the solid–liquid interface. The governing equations of the dimensionless concentration u and the nonconserved order parameter φ at a fixed temperature are as follows:

$$\tau_\varphi(\theta)\frac{\partial\varphi}{\partial t} = \nabla\left[W^2(\theta)\nabla\varphi\right] + \sum_i^{x,y}\partial_i\left[|\nabla\varphi|^2\frac{\partial W^2(\theta)}{\partial(\partial_i\varphi)}\right] + \varphi - \varphi^3 - \lambda\left(1-\varphi^2\right)^2 u, \tag{1}$$

$$\left[\frac{1+k(T)}{2} - \frac{(1-k(T))\varphi}{2}\right]\frac{\partial u}{\partial t} = \boldsymbol{\nabla}\cdot\left[D_l q(\varphi)\boldsymbol{\nabla}u - \boldsymbol{J}_{\mathrm{AT}}\right] + \frac{1}{2}\left[1+(1-k(T))u\right]\frac{\partial\varphi}{\partial t}, \tag{2}$$

with

$$u = \frac{2k(T)c/[c_0(1+k(T)) - c_0(1-k(T))\varphi] - 1}{1-k},$$

$W(\theta) = W_0 a_{\mathrm{s}}(\theta)$, and $\tau_\phi(\theta) = \tau_0 a_{\mathrm{s}}^2(\theta)[1+(1-k(T))u]$, where c_0 is the alloy concentration, $k(T)$ is the temperature dependent partition coefficient,

$$\boldsymbol{J}_{\mathrm{AT}} = W_0/2\sqrt{2}[1+(1-K)U]\partial_t\phi\boldsymbol{\nabla}\phi/|\boldsymbol{\nabla}\phi|$$

is the anti-trapping current term that can recover precisely local equilibrium at the interface, $a(\theta) = 1 + \varepsilon_4\cos 4\theta$ is the anisotropic function, θ is the angle between the direction of the temperature gradient and the direction normal to the solid–liquid interface, ε_4 is the fourfold interface energy anisotropic strength, $q(\varphi) = (1-\varphi)/2$ is an interpolation function, D_{l} is the liquid diffusivity which is assumed to be independent of the temperature, and the solid diffusivity D_{s} is neglected because the liquid diffusivity is three orders of magnitude higher than the solid diffusivity in the alloy system. The time scale τ_0 and the characteristic length W_0 are related to capillary length and liquid diffusion coefficient, where $W_0 = \lambda d_0/a_1$ and $\tau_0 = \lambda a_2 W_0^2/D_{\mathrm{l}}$, $a_1 = 0.8839$ and $a_2 = 0.6267$, where λ is a coupling parameter determining the width of the solid–liquid interface in the simulated system, where d_0 is the capillary length obtain by $d_0 = \Gamma/|m_{\mathrm{l}}(T)|(1-k(T))c_{\mathrm{l}}^{\mathrm{eq}}(T)$, where $k(T)$ is the partition coefficient, $c_{\mathrm{l,s}}^{\mathrm{eq}}(T)$ is the equilibrium liquid and/or solid concentrations, $m_{\mathrm{l}}(T)$ is the slope of the liquidus curve , and hence the capillary length d_0 is certainly a function of the given temperature T.

In this study, we selected the well-characterized Al–4 wt.% Cu alloy as the simulation object, and the phase diagram of the aluminum-rich portion in aluminum-copper system is shown in Fig. 1(a). We focus on the dendritic growth in three values of temperature $T = 898$ K, 888 K, and 878 K, corresponding to the initial supersaturation $u_0 = -0.767$, -0.849, and $u_0 = -0.898$. We calculated $k(T)$, $c_{\mathrm{l,s}}^{\mathrm{eq}}(T)$, and $m_{\mathrm{l}}(T)$ according to data from the phase diagram. Moreover, the liquid diffusivity D_{l} is fixed at $D_{\mathrm{l}} = 3000$ μm^2/s. In the quantitative phase-field model, the computational accuracy increases

with decreasing W_0, but the decrease of W_0 leads to the incredible increase of the computational cost. For balancing accuracy and efficiency of numerical simulations, we selected $\lambda = 0.75$, $\lambda = 1.2$, and $\lambda = 2$ for $T = 898$ K, 888 K, and 878 K, respectively. Equations (1) and (2) are solved by using the finite difference method, and no-flux boundary conditions are applied to all boundaries. Note that dendritic tip shape can be affected by the accumulated solute when the computation domain ahead of the dendrite tip is too short. To avoid that, the simulation domain is 1200×1200. We initialize a solid nucleus at the center of the computational domain, as shown in Fig. 1(b). The grid spacing for 898 K, 888 K, and 878 K is $\Delta x/W_0 = 0.6$, $\Delta x/W_0 = 0.5$, and $\Delta x/W_0 = 0.4$, respectively, while the time steps are $\Delta t/\tau_0 = 0.008$, $\Delta t/\tau_0 = 0.006$ and $\Delta t/\tau_0 = 0.005$, respectively. In most alloys systems, the preferred crystalline growth directions of a dendrite are a result of the interfacial energy anisotropy. In this work, we aimed to study the effect of the interface energy anisotropic strength on the dendritic tip selection during solidification of alloys, and hence ε_4 is varied from 0.01 to 0.04 although ε_4 is about 0.01 for aluminum-based alloys. Note that although the system is isothermal in this study, this model can be applied to the non-isothermal solidification through introducing the thermal field equation or setting the system temperature as a function of time combined with a constant cooling rate.

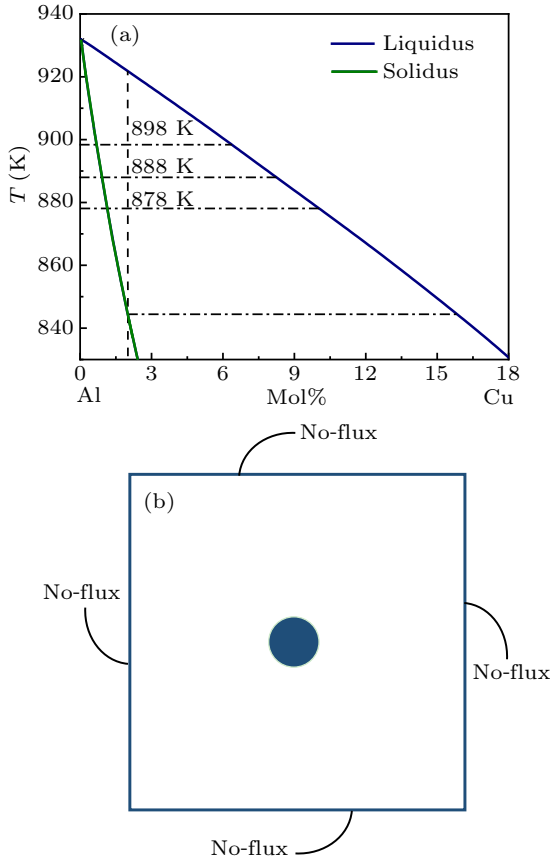


Fig. 1. (a) Phase diagram of Al–Cu alloy; (b) schematic of numerical domain and boundary conditions.

3. Numerical results and discussion

Because the growth morphology and concentration field distributions of the isometric crystals at $\Delta T = 23$ K, 33 K, 43 K are similar, to avoid redundancy we plotted the dendritic morphologies and concentration field distributions for dendrite growth at $\Delta T = 33$ K for various the interface energy anisotropy parameters ε_4 at the same time, as shown in Fig. 2(a). Note that although it is unusual for $\varepsilon_4 > 0.02$ in the aluminum alloys system, the characteristic of the dendritic tip selection with the interface energy anisotropy is unclear. Clearly, the interface energy anisotropy plays a crucial role in dendritic tip selection, i.e., the increase of the interface energy anisotropy results in the sharper dendritic tip and faster dendritic tip velocity. The dendritic tip radius, the key characteristic parameter of dendritic shape, is determined by fitting the $\varphi = 0$ contour profile to a parabolic function with a fourth-order interpolation scheme. Fitting the equation with a parabola $y = Ax^2 + Bx^4$, where A and B are fitting parameters, and thus $\rho = 1/(2A)$ and $A_4 = B\rho^3$. According to previous experimental and numerical investigations,[7,25] the value of the tip radius depends on the fitting range. In order to investigate the evolution of the fitted tip radius with the fitting range, we carried out a series of polynomial fittings, and an example of the case of $\varepsilon_4 = 0.02$ is shown in Fig. 2(b). The results of ρ and A_4 are presented in Fig. 3. It can be seen from Fig. 3(a) that the obtained tip radius increases and then stabilizes with the increase of the fitting range for all cases, and greater anisotropy parameter results in a smaller tip radius. Figure 3(b) illustrates that the fourth-order amplitude coefficient A_4 varies with the increase of the fitting range. In all the cases, A_4 decreases with the fitting range increasing, which is in agreement with the experimental results.[7] It can be observed that A_4 finally stabilized to about 0.00161, 0.00119 and 0.00126, with the increase of the fitting range for all cases of ε_4 for $\Delta T = 23$ K, $\Delta T = 33$ K and $\Delta T = 43$ K, respectively. Therefore, it seems that A_4 is independent of ε_4 and ΔT, at least in the present range of ΔT. The effect of the undercooling on the fourth-order amplitude coefficient A_4 warrants further investigations.

Figure 4 shows that the growth velocity of dendritic tip varies with the increase of ε_4 for three different undercoolings. It is obvious that for all cases of undercooling, the stronger the anisotropy, the faster the tip growth velocity, and this phenomenon is more obvious at high undercooling. Based on the results discussed above, the relationship between the steady-state growth rate V and radius ρ of the dendrite tip for various values of ε_4 can be derived. Combined with ρ and V, we can calculate the tip selection constant σ^* according to the definition $\sigma^* = 2Dd_0/(\rho^2 V)$. Figure 5 shows the tip selection constant σ^* with the variation of fitting range for $\varepsilon_4 = 0.01$, 0.02, 0.03, 0.04 for three different undercoolings. Clearly,

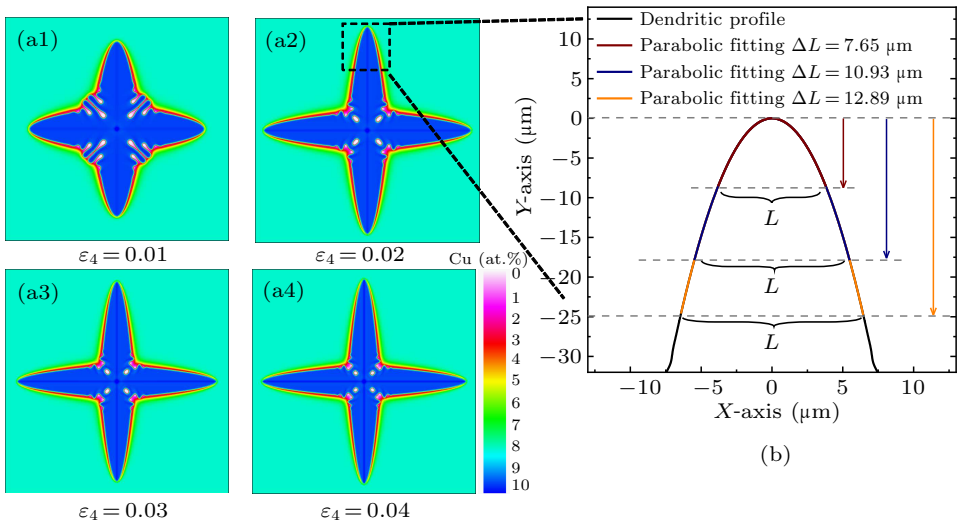


Fig. 2. (a) Dendritic morphologies for $\varepsilon_4 = 0.01$, 0.02, 0.03, 0.04 at $\Delta T = 33$ K at a fixed time; (b) schematic of fitting dendritic profile to a parabolic function with a fourth-order interpolation for $\varepsilon_4 = 0.02$.

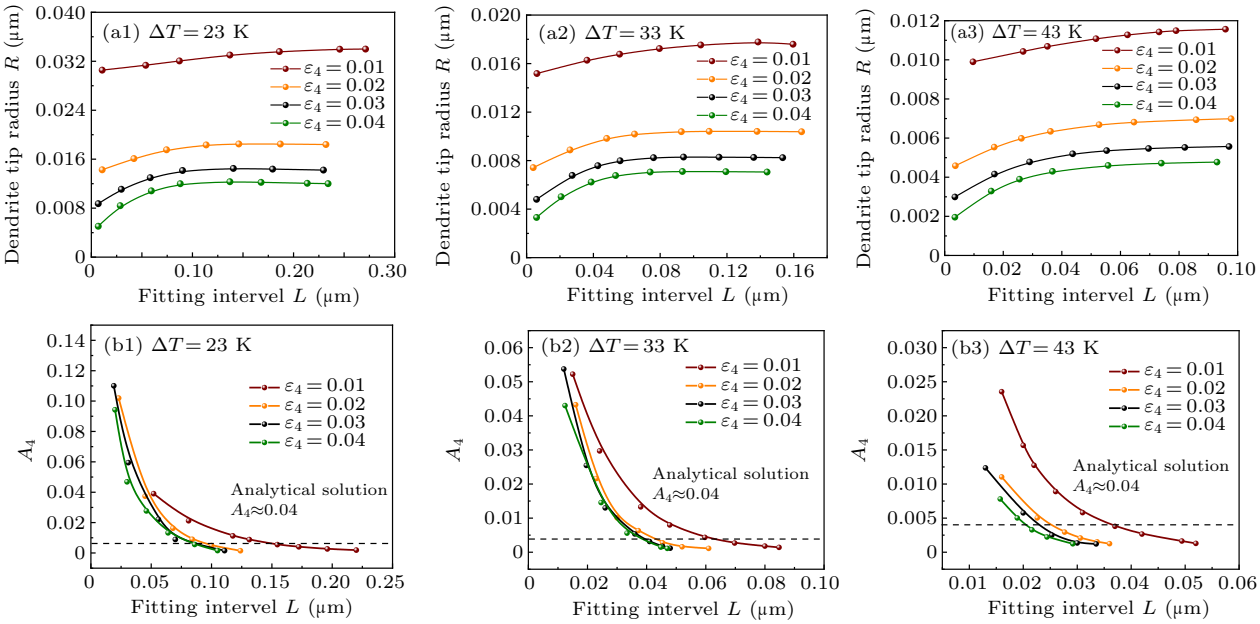


Fig. 3. Tip radius (a) and fourth-order amplitude coefficient A_4 (b) obtained from the parabolic function with the variation of fitting range for $\varepsilon_4 = 0.01$, 0.02, 0.03, 0.04.

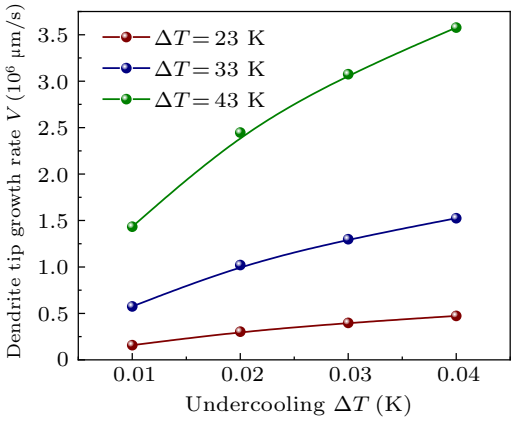


Fig. 4. Tip growth velocity V is a function of interface energy anisotropy parameter ε_4 for three different undercoolings.

σ^* decreases and then stabilizes with the increase of the fitting range for all cases, and σ^* increases with the increase of ε_4. According to MST,[2] σ^* depends on ε_4, having $\sigma^* \propto \varepsilon_4^{7/4}$ in the low undercooling regime. Although the undercooling used in our simulations is rather large compared with previous investigations,[2] the relationship between σ^* and ε_4 follows a similar power-law function. Figure 6 shows results by fitting numerical data with $\sigma^* \propto \varepsilon_4^{\alpha}$ for various fitting ranges. Interestingly, the fitting parameter α depends strongly on the fitting range L/W_0, as shown in Fig. 6(b). For $L/W_0 = 5.5$, $\alpha = 1.97$, 1.83, and 1.90, correspond to $\Delta T = 23$ K, 33 K and 43 K, respectively. The values of α are close to 7/4 from MST.[4] However, for $L/W_0 = 130$, $\alpha = 0.67$, 0.60, and 0.67, correspond to $\Delta T = 23$ K, 33 K and 43 K, respectively. Therefore, α is independent of ΔT but dependent of L/W_0.

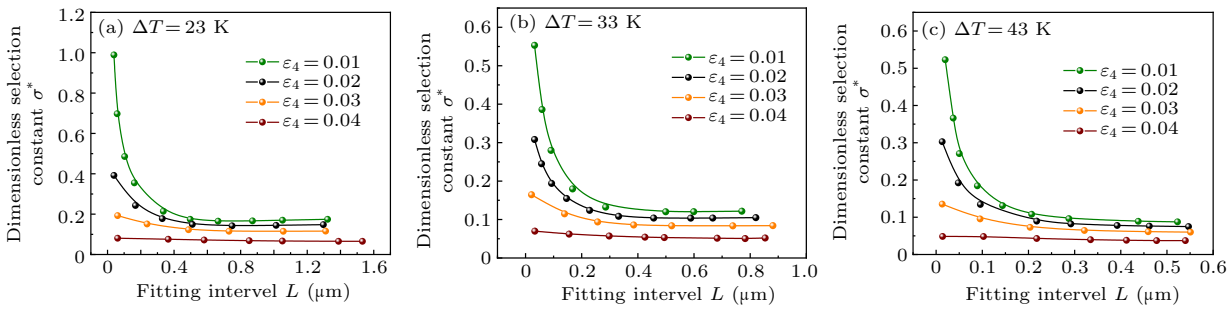


Fig. 5. Tip selection constant σ^* with the variation of fitting range for $\varepsilon_4 = 0.01$, 0.02, 0.03, 0.04 for three different undercoolings.

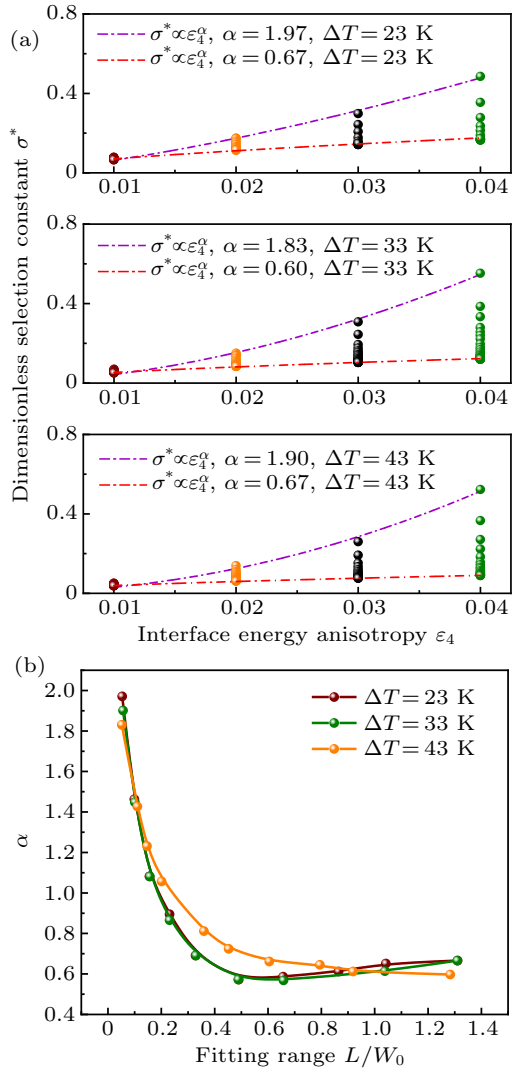


Fig. 6. (a) The power-law relationship between the tip selection constant σ^* and the interface energy anisotropy parameter ε_4 for various undercoolings; (b) α varies with the fitting range for various undercoolings.

The values for σ^* obtained from our numerical simulations for various undercoolings and interface energy anisotropy parameters are compared to the experimental results and MST in Fig. 7. The MST curve is plotted in the solid line, while the dashed line represents an approximate extension line of the MST curve, following the power-law relationship $\sigma^* \propto /4$. It can be seen that the values of σ^* measured for real alloys, such as an Al–Cu alloy[8] and a Ga–In alloy,[2] are in excellent agreement with MST. For transparent alloys, the value of σ^* obtained from NH_4Br-H_2O[2] falls almost exactly on the MST line, whereas the value from SCNACE[7] is significantly larger than that on the MST line. Our numerical results from phase-field simulations are plotted in the circle, and the vertical bar indicates the range of values measured for various fitting ranges. It can be seen that our results are close to the MST line for $\varepsilon_4 < 0.02$, while the size of the vertical bar becomes larger with the increase of ε_4. Clearly, the predicted σ^* obtained from our phase-field simulations is sensitive to the undercooling when ε_4 is fixed. It should be noted that the definition of the tip selection constant σ^* is obtained in MST for the cubic crystal system of the present study. The definition of the tip selection constant σ^* in MST is the same as that of the hexagonal crystal system studied by Duan *et al.*[26]

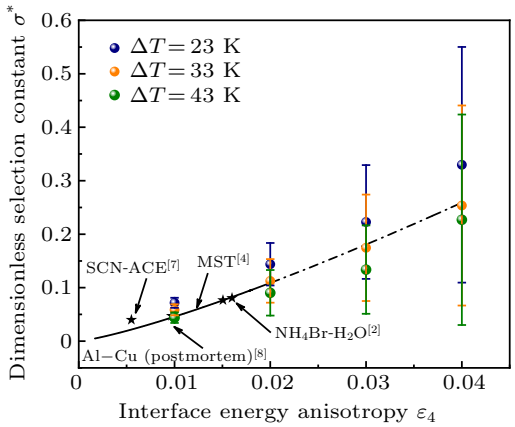


Fig. 7. Dendrite tip selection parameters σ^* versus interfacial energy anisotropy parameter ε_4.

4. Conclusion

In this paper, we numerically investigated the effect of undercooling ΔT and the interface energy anisotropy parameter ε_4 on the shape of the equiaxed dendritic tip by developing the quantitative phase-field model for solidification of binary alloys. It was found that larger ε_4 leads to sharper dendritic tips and faster tip growth velocity. The tip radius ρ calculated by fitting the $\varphi = 0$ contour profile to a parabolic function with a fourth-order interpolation scheme gradually increases and then stabilizes with the increases of the fitting range while A_4 decreases and then stabilizes. The results show that A_4 is

independent of ε_4 and ΔT. It is observed that as the fitting range increases, the dendrite tip shape selection parameter σ^* decreases and then stabilizes. Additionally, a larger value of ε_4 corresponds to a larger value of σ^*. We found that the relationship between σ^* and ε_4 still follows a power-law function $\sigma^* \propto \varepsilon_4^{\alpha}$, and the fitting parameter α depends strongly on the fitting range L/W_0. Furthermore, our results align with the MST curve[2] when ε_4 is less than 0.02. Notably, the predicted value of σ^* obtained from our phase-field simulations is sensitive to the undercooling, particularly when ε_4 is fixed.

Acknowledgements

Project supported by the National Key Research and Development Program of China (Grant No. 2021YFB3502600) and Shenzhen Science and Technology Program (Grant No. JCYJ20220530161813029).

References

[1] Zhao Y, Zhang B, Hou H, Chen W and Wang M 2019 *J. Mater. Sci. Technol.* **35** 1044
[2] Neumann-Heyme H, Shevchenko N, Grenzer J, Eckert K, Beckermann C and Eckert S 2022 *Phys. Rev. Mater.* **6** 063401
[3] Dantzig J A and Rappaz M 2016 *Solidification* 2nd Edn. (Lausanne: EPFL Press) p. 319
[4] Kurz W, Fisher D J and Trivedi R 2019 *Int. Mater. Rev.* **64** 311
[5] Chopra M, Glicksman M and Singh N 1988 *Metall. Trans. A* **19** 3087
[6] Li Q and Beckermann C 2002 *J. Cryst. Growth* **236** 482
[7] Melendez A J and Beckermann C 2012 *J. Cryst. Growth* **340** 175
[8] Liu S, Li J, Lee J and Trivedi R 2006 *Philos. Mag.* **86** 3717
[9] Kurz W, Rappaz M and Trivedi R 2021 *Int. Mater. Rev.* **66** 30
[10] Dougherty A and Lahiri M 2005 *J. Cryst. Growth* **274** 233
[11] Zhao Y, Xing H, Zhang L, Huang H, Sun D, Dong X, Shen Y and Wang J 2023 *Acta Metall. Sin. (Engl. Lett.)* **36** 1749
[12] Zhu J H, Zhen L, Zhong B Y, Wang Y J and Xu B X 2023 *Chin. Phys. B* **32** 47701
[13] Zhu C S, Guo Z H, Lei P, Feng L and Zhao B R 2022 *Chin. Phys. B* **31** 68102
[14] Shen X and Wang Q 2022 *Chin. Phys. B* **31** 48201
[15] Li Y N, Hai M M, Zhao Y, Lv Y L, He Y, Chen G, Liu L Y, Liu R C and Zhang G G 2018 *Chin. Phys. B* **27** 128703
[16] Chen W P, Hou H, Zhang Y T, Liu W and Zhao Y H 2023 *Chin. Phys. B* **32** 118103
[17] Chen L Q and Zhao Y 2022 *Prog. Mater. Sci.* **124** 100868
[18] Zhao Y 2023 *npj Comput. Mater.* **9** 94
[19] Karma A and Rappel W J 1998 *Phys. Rev. E* **57** 4323
[20] Karma A and Lee Y H 2000 *Phys. Rev. E* **61** 3996
[21] LaCombe J, Koss M, Fradkov V and Glicksman M 1995 *Phys. Rev. E* **52** 2778
[22] Rosam J, Jimack P K and Mullis A M 2009 *Phys. Rev. E* **79** 030601
[23] Mullis A M, Rosam J and Jimack P K 2009 *Trans. Indian Inst. Met.* **62** 309
[24] Ramirez J C, Beckermann C, Karma A and Diepers H J 2004 *Phys. Rev. E* **69** 051607
[25] Xing H, Dong X, Wang J and Jin K 2018 *Metall. Mater. Trans. B* **49** 1547
[26] Duan P P, Xing H, Chen Z, Hao G H, Wang B H and Jin K X 2015 *Acta Phys. Sin.* **64** 060201 (in Chinese)